

Mississippi State University

Scholars Junction

College of Arts and Sciences Publications and
Scholarship

College of Arts and Sciences

2003

Patterning and Imaging of Oxides on Glassy Carbon Electrode Surfaces by Scanning Electrochemical Microscopy

David O. Wipf

Mississippi State University, dow1@msstate.edu

Robert C. Tenent

Follow this and additional works at: <https://scholarsjunction.msstate.edu/cas-publications>

Recommended Citation

Wipf, David O. and Tenent, Robert C., "Patterning and Imaging of Oxides on Glassy Carbon Electrode Surfaces by Scanning Electrochemical Microscopy" (2003). *College of Arts and Sciences Publications and Scholarship*. 25.

<https://scholarsjunction.msstate.edu/cas-publications/25>

This Preprint is brought to you for free and open access by the College of Arts and Sciences at Scholars Junction. It has been accepted for inclusion in College of Arts and Sciences Publications and Scholarship by an authorized administrator of Scholars Junction. For more information, please contact scholcomm@msstate.libanswers.com.

Patterning and Imaging of Oxides on Glassy Carbon Electrode Surfaces by Scanning Electrochemical Microscopy

Robert C. Tenent^a and David O. Wipf^{*z}

Department of Chemistry, Box 9573, Mississippi State University,

Mississippi State, MS 39762, USA

Abstract

The scanning electrochemical microscope is used to form and characterize patterns of oxides on glassy carbon surfaces. Chemically specific imaging of oxides present on these surfaces was demonstrated by taking advantage of differential heterogeneous electron-transfer rates for the Fe(II/III) reaction occurring at unoxidized and oxidized glassy carbon electrodes. Localized generation of surface oxides was demonstrated using both the micro-reagent and direct modification modes of SECM. The micro-reagent mode was used to perform a chemical oxidation of the surface by generating the strong oxidant Ag(II) at the UME tip while positioned close to the carbon surface, however, this technique was found to have poor reproducibility. Direct mode oxidation was found to be a much more versatile route toward the generation of complex patterns of oxides on carbon surfaces. The reproducibility of the direct mode technique was found to depend heavily on solution resistance. “Charge dose” studies, followed by reaction-rate imaging, qualitatively show that the electron-transfer rate for the Fe(II/III) system scales with the amount of charge “injected” in each oxidation experiment, indicating a correlation between surface oxide density and electron-transfer rate.

Submitted, J. Electrochem. Soc., March 12, 2002, Revised August 14, 2002

^a Present address: ZettaCore, Inc., 920 Main Campus Drive, Suite 400, Raleigh, NC 27606

^{*} Electrochemical Society Member

^z wipf@ra.msstate.edu

The presence of surface oxides on carbon electrodes plays a major role in their use in electrochemistry. Oxides act as precursor sites for further derivatization of the electrode surface¹⁻⁵ and have been implicated as electron-transfer catalysts for a number of reactions.⁵⁻¹⁵ Initial studies measured carbon-to-oxygen-ratios using XPS before and after surface treatments.^{10,11,16-22} While these experiments gave information about the relative amount of oxides before and after a particular treatment, they gave limited information about surface heterogeneity or the type of oxides formed. McCreery and co-workers have extensively studied oxides on carbon electrode surfaces using Raman spectroscopy.²³⁻²⁵ This has enabled workers to examine not only the presence of oxides on the electrode surface, but also to label specific types of oxides with Raman active compounds.^{23,25} A scanning Raman instrument was used to image structural heterogeneity of glassy carbon electrodes and to distinguish oxide sites by detecting the chemisorption of dinitrophenylhydrazine.²⁴ Kuhr's research group used fluorescence microscopy to observe the distribution of oxides on carbon-fiber ultramicroelectrodes by attaching fluorescein-labeled latex beads to oxide sites through carbodiimide and biotin-avidin chemistries.²⁶⁻²⁸

While these techniques have proven useful for studies of surface structure and the presence of a variety of oxides, several of them require surface modification and they do not directly examine electron-transfer reactions occurring at specific sites. The scanning electrochemical microscope (SECM) can directly examine electrochemical events occurring *in situ* on electrode surfaces at sub-micrometer resolution without the need for derivatization of the surface. SECM is a scanned probe microscope that uses an ultramicroelectrode (UME) as an imaging tip. Imaging capabilities are based on electrochemical phenomena occurring in

an electrolyte solution between a UME tip and a sample surface. This is often accomplished with an intentionally added solution species that mediates electron transfer, et, between the tip and substrate. For a detailed discussion of the technique, the interested reader is referred to a recent monograph²⁹ and other recent reviews.³⁰⁻³²

The present work shows that SECM can be used to perform selective oxidation at predetermined sites as well as chemically specific imaging of oxides on the surface of glassy carbon electrodes. Chemically specific imaging is accomplished with the “reaction-rate” imaging mode, which uses an et mediator species having a heterogeneous et rate that is sensitive to the presence of oxides on the electrode surface. The reaction-rate mode was first described by Wipf and Bard³³ and is designed to image the reactivity of a substrate surface with respect to a chosen SECM mediator species. In positive-feedback imaging with SECM, the electron-transfer processes occurring between the mediator and the tip and substrate electrodes must be mass-transport limited. Under these conditions, the tip current is a function of the distance the mediating species must travel between the tip and substrate and thus images are of the sample topography. Reaction-rate mode imaging is performed with the tip at the mass-transport limit, while the rate of et from the substrate to the mediator at the substrate is kinetically limited. Under these conditions, the tip current depends not only on the distance between the tip and the substrate surface, but also on the rate of the et reaction as it occurs at the substrate surface. Therefore, the tip current becomes a direct measure of surface reactivity. The separate effects of heterogeneous electron-transfer kinetics and topography can be deduced by imaging under conditions where the mediator-substrate reaction occurs at different rates, such as by varying the substrate potential or changing the

mediator. Alternately, the tip-to-substrate distance can be independently determined by use of a constant-separation method that does not rely on the SECM tip current for positioning.³⁴⁻³⁹

The initial example of the reaction-rate mode demonstrated the selective imaging of gold embedded in a glassy carbon matrix by taking advantage of the difference in heterogeneous electron-transfer rates for the Fe(II/III) system on gold and carbon surfaces. Gold surfaces show much faster heterogeneous et than glassy carbon for the Fe(II/III) species.⁴⁰ Under appropriate conditions the much higher reactivity towards Fe(II/III) et reactions leads to selective imaging of gold regions.

A similar example of reaction-rate mode is the imaging of a colloidal carbon film sprayed (by aerosol⁴¹) on gold using ferrocenemonocarboxylic acid as the et mediator.⁴² Schuhmann and co workers demonstrated imaging of intentionally introduced pinholes in alkanethiolate monolayers based on differences in et kinetics for the ferri/ferrocyanide redox couple between bare gold and thiolate monolayer coated surfaces.⁴³ Recently, Hillier and coworkers have used reaction-rate mode to study processes occurring on platinum surfaces.⁴⁴⁻⁴⁶ Reaction-rate imaging is not limited to electronically conducting surfaces. A number of authors have demonstrated reaction-rate imaging of enzyme activity in various substrates.⁴⁷⁻⁵⁰ In these experiments, the enzyme-mediator reaction is kinetically limited.

SECM can also be used as a versatile tool for the localized modification of electrode surfaces through two distinct modes. The first is the micro-reagent mode that uses the tip electrode to generate a reactive species near an electrode surface. Some examples of micro-reagent mode modifications are the patterning of biotin on glassy carbon electrode

surfaces,⁵¹ the deposition of metals into polymer films by reducing metal ions inside the film with solution phase species generated at the tip,⁵² and local deposition of polyaniline patterns on various electrode surfaces by using the tip electrode to locally change solution pH.⁵³ The second is the direct mode that uses the tip to direct a localized flow of current through the substrate surface. Some examples of direct mode modifications are the localized reductive desorption of alkane-thiolate self-assembled monolayers on gold,⁴³ and the deposition of two-dimensional⁵⁴ and three-dimensional⁵⁵ polypyrrole structures. We have recently demonstrated both micro-reagent and direct mode modifications of carbon fiber UME's to fabricate immobilized enzyme electrodes.⁵⁶

Here we perform localized oxidations on larger glassy carbon electrodes using both the micro-reagent and direct modification modes. Micro-reagent mode is used to drive a local chemical oxidation by generating a strong oxidizing agent at an SECM tip electrode in the immediate vicinity of a carbon substrate. The direct mode is used to drive a localized direct electrochemical oxidation of the carbon surface by passing current between closely spaced tip and substrate electrodes. The ability to generate local regions of oxides on carbon surfaces and characterize them is useful for two reasons. As mentioned previously, the locally generated oxides can function as tethering sites for further modification thereby allowing sequential modification of predetermined regions on the same surface. In addition, the ability to generate oxides at specific sites on the surface also allows for the direct examination of et reaction catalysis by providing a direct comparison between the oxidized and unoxidized regions of the same surface. This is useful because multiple experiments can be conducted on

a single sample, which eliminate the variances in electrode performance commonly caused by surface preparation techniques.^{57,58}

Experimental

Reagents Iron (II) and (III) perchlorate hydrate was purchased from Aldrich Chemical (Milwaukee, WI). All other chemicals were ACS reagent grade and used as received.

Solutions were prepared from 18 M Ω ultra-pure water (Milli-Q, Millipore Corp., Bedford, MA). All solutions were stored at room temperature and were not deoxygenated before use.

Electrodes 3 mm dia. glassy-carbon and Ag/AgCl reference electrodes were purchased from Bioanalytical Systems, Inc. (West Lafayette, IN). The glassy carbon electrodes were prepared by polishing with a slurry of 0.05 μm alumina particles suspended in deionized water using a felt pad on a polishing wheel. No special attempts were made to employ electrode preparation techniques that have been shown to generate surfaces with either high or low naturally occurring oxides.

Mercury/mercury sulfate and saturated calomel reference electrodes were constructed in house using previously published procedures.⁵⁹ Although several different reference electrodes were used throughout the course of this work, all potentials are reported versus the Ag/AgCl reference scale. SECM tip electrodes were manufactured using both 10- μm and 100- μm dia. Pt wires and 12.7- μm dia. Au wire using previously published procedures.^{60,61}

Experimental Apparatus The SECM used in this work has been described previously.⁶² A brief explanation is given here. The tip and substrate potentials are independently controlled versus a single reference electrode by a bipotentiostat (EI-400, Ensmann Instruments, Bloomington, IN). Tip movement is controlled by a micro-positioning

system that consists of three "inchworm" positioning motors (Burleigh, Fisher, NY) that are driven by the Burleigh 6000 system controller. The positioning motors and translation stages are built into a single assembly and placed on a vibration isolation table (Newport, Irvine, CA). A personal computer controls the tip positioning and data collection using software written in house. The SECM cell consists of a small Teflon cup. The bottom of the cell has an opening for placement of the substrate electrode and a small plastic plate with access holes was screwed in to the top of the cell assembly to hold the reference and auxiliary electrodes.

Tip placement for all SECM images shown was performed by approaching under positive feedback conditions until the tip current was twice the value measured in bulk solution. At this point, the tip to substrate distance is approximately half of the tip radius.

Cyclic voltammetry experiments were conducted using the BAS 100B/W Electrochemical workstation (Bioanalytical Systems, West Lafayette, IN). Background subtractions for cyclic voltammetric experiments were conducted by collecting nine voltammograms in the chosen electrolyte in the absence of electro-active species. These scans were averaged using the BAS software package and subtracted from voltammograms taken under identical conditions in the presence of the electroactive species of interest. The background signal in blank electrolyte often changed slightly in the first few scans and became more reproducible thereafter.

Optical microscopy was performed with an Olympus BH-2 microscope (Olympus, Lake Success, NY) fit with 5X, 10X, 20X and 50X objectives. Photomicrographs were taken with a digital camera (Pixera Professional, Pixera Corp., Los Gatos CA) mounted on the trinocular head.

The direct-mode oxidation of the carbon surface was performed using a home-built galvanostat that permits constant currents ranging from 1 nA to 1 mA to pass between the tip and substrate electrodes.⁶³ The galvanostat was constructed to allow remote-controlled switching between potentiostat control (using a bipotentiostat) and galvanostatic control without disturbing the tip or substrate electrode connections. A timing circuit was used to switch the galvanostat on and off after precise times in order to give reproducible charge dosages for the oxidation procedure.

Results and Discussion

Imaging of Oxides on Glassy Carbon with Reaction-Rate Mode SECM The procedure for reaction-rate imaging of oxides on carbon surfaces is based on the distinctive behavior of the Fe(II/III) redox couple on a glassy-carbon electrode (GCE). Several authors have noted that an oxidative treatment of a GCE increases the heterogeneous et rate for the Fe(II/III) system.^{10,14,15,64} Chen and McCreery, in particular, have demonstrated that the electrocatalysis of the Fe(II/III) reaction is directly related to the presence of carbonyl groups on the surface.^{7,8} Fig. 1 shows background subtracted cyclic voltammograms for a 3 mm GCE in a solution of 1 M H₂SO₄ with 2 mM Fe(II) perchlorate both before and after an electrochemical pretreatment consisting of three potential cycles from 0.00 to 2.20 V vs. Ag/AgCl in a solution of 1 M H₂SO₄. The large decrease in the peak separation upon oxidation is indicative of accelerated et kinetics.⁶⁵ The difference in kinetics for the iron et reaction occurring at unoxidized and oxidized glassy carbon can be used to selectively image

regions of oxide on these surfaces in the same manner as described for the gold/glassy carbon system of Wipf and Bard.³³

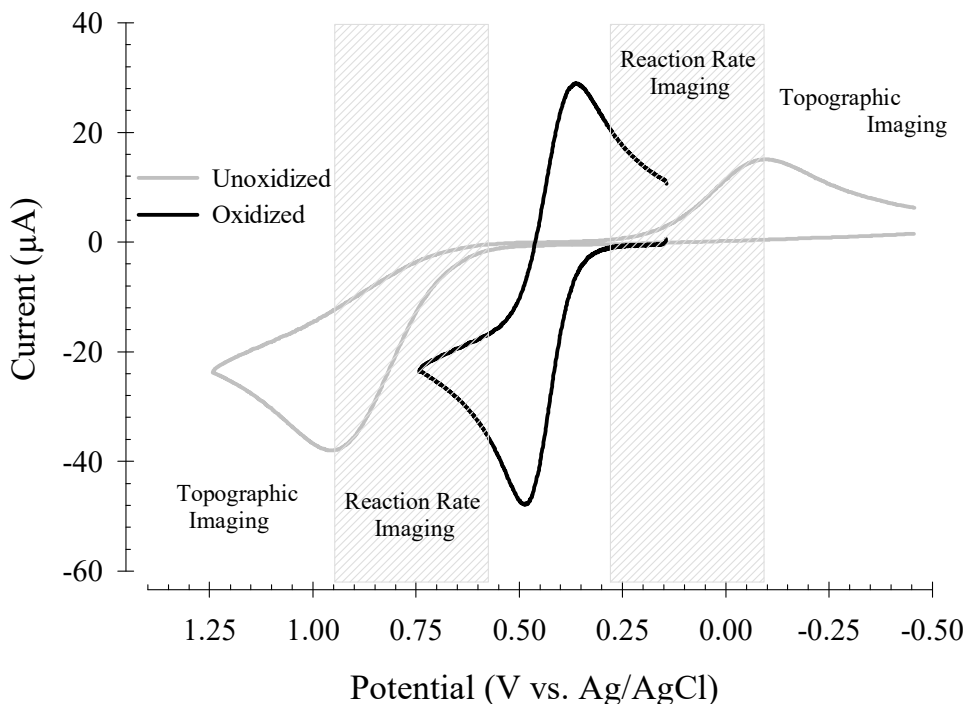


Fig. 1. Background subtracted cyclic voltammetry for a 3 mm GCE in a cell containing 2 mM $\text{Fe}(\text{ClO}_4)_2$ in 1 M H_2SO_4 before and after an intentional electrochemical oxidation of the electrode surface. 100 mV/s scan rate. The shaded regions indicate regions of applied substrate potentials suitable for use in reaction-rate imaging mode. The oxidation procedure is described in the text.

Regions of applied substrate potentials suitable for both reaction-rate and topographic imaging use are labeled in fig. 1. In all cases, the tip electrode is biased for a diffusion-limited process (0.80 V for the oxidation of Fe(II) to Fe(III)). Fig. 1 shows that a large window of applied potentials exists for the substrate to reduce Fe(III) to Fe(II) (~0.25 V to -0.10 V, the right-most shaded region in the figure) in which an oxidized carbon surface is at or close to the mass-transport limit while the unoxidized region is kinetically limited. In this

region of applied substrate potentials, the regeneration of Fe(II) from the Fe(III) generated at the tip electrode will be very fast in the oxidized regions of the surface, but still kinetically limited in the unoxidized regions. This will lead to increased tip current due to faster mediator regeneration with the tip over oxidized regions and decreased tip current due to slower mediator regeneration over unoxidized regions. As the potential of the substrate electrode is moved to more extreme potentials (< -0.10 V), a purely topographic image is obtained since the et rate at the unoxidized surface increases to the mass transport limit. This phenomenon makes selective imaging of oxides on carbon surfaces using the reaction-rate mode possible. Note that the Pt tip electrode shows much faster et kinetics for the Fe(II)/(III) reaction⁴⁰ and thus the extreme potentials to drive the process on the carbon surface at a mass-transport limit are not necessary.

While the example voltammograms shown here are for the oxidation of Fe(II) to Fe(III), this scheme is also valid for the reverse reaction of the reduction of Fe(III) to Fe(II). With the reduction of Fe(III) occurring at the tip electrode, the substrate would be biased in the region from approximately 0.60 V to 1.00 V as also shown in fig. 1.

Fig. 2 includes reaction-rate images of a partially oxidized GCE. The images were collected at the border between regions of oxidized and unoxidized carbon in a solution of 2 mM Fe(ClO₄)₃ in 1 M H₂SO₄ with a 10- μ m dia. Pt tip electrode. In this example, the tip electrode is biased at 0.00 V to drive the diffusion-limited reduction of Fe(III) to Fe(II) and the substrate potentials were varied between 0.80 V (reaction-rate imaging) and 1.40 V (topographic imaging). Partial oxidation of the surface was accomplished by masking half of the GCE surface with Teflon tape before exposing it to the same oxidation procedure described previously. Separate control experiments showed that the Teflon masking

procedure had a negligible effect on the carbon electrode surface. The current scale in these images is the normalized tip current ($I_t = i_t/i_{t,\infty}$), where i_t is the acquired tip current and $i_{t,\infty}$ is the tip current at a large distance from the substrate, i.e. about 20 tip diameters.

Accompanying the image data are line-scan data of I_t vs. distance, extracted from each image at the location of the dashed line. The left side of each image is the region of the surface that had been exposed to the oxidation procedure and the right side is the region that was protected by the Teflon tape mask. Figs. 2A-B are collected under reaction-rate imaging conditions and show an increase in current on the oxidized portion of the surface relative to the unoxidized as expected. As the applied potential increases, the response shifts from kinetic to topographic due to the overall increased et rate on the entire surface. As discussed previously, under reaction-rate conditions, the tip current depends on both the tip-substrate separation and on the electron-transfer rate at the substrate surface. In fig. 2A, the et rate at the unoxidized substrate surface is sufficiently slow to mimic the behavior of an insulating surface. An insulating surface blocks mass transport of solution species from the tip electrode, producing a decrease in tip current upon approach. Note, however, that the unoxidized substrate in 2A retains some et activity since the current is higher than expected for a strictly insulating region. At larger heterogeneous et rates (compare the oxidized region of 2A or the unoxidized region in 2D), regeneration of the mediator species at the substrate occurs, increasing the tip current upon approach. In general, I_t will be less than unity at a kinetically slow electrode and greater than unity at a kinetically rapid surface. This is consistent with the slow and rapid kinetics expected at the unoxidized regions of figs. 2A and 2D. The response of figs. 2B and 2C are intermediate between these extremes.⁶⁶

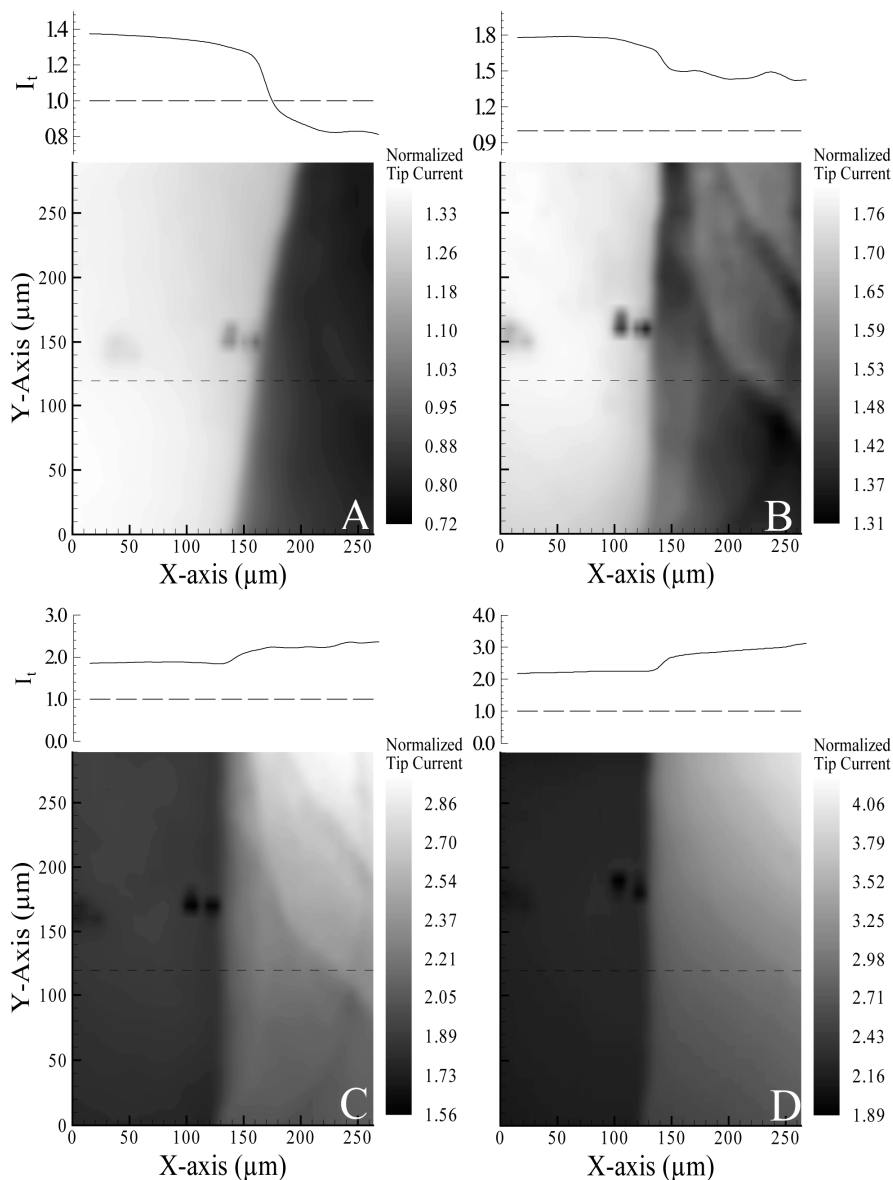


Fig. 2. SECM reaction-rate mode images of a partially oxidized glassy carbon surface. These images were collected at the border between oxidized and unoxidized regions. The procedure for partial oxidation is described in the text. The left side of each image is oxidized carbon and the right is unoxidized. Tip potential was 0.00 V and substrate potentials were (A) 0.80, (B) 1.00, (C) 1.20, and (D) 1.40 V vs. Ag/AgCl. Extracted line scan data is shown above each image. The line scan data was extracted from the region marked by the dotted line in each image.

Several interesting features of these images also indicate that the observed response is not described strictly by topographic arguments. Considering only the oxidized region of figs. 2A-D, the line scan data indicate that the current is greater than unity on all images but increases with potential. This indicates, at least for figs. 2A-2C, that et rates on the oxidized region are not at the diffusion limit and thus are controlled in part by et kinetics. However, according to the voltammogram in fig. 1, these images should have mass-transport limited et rates. This is likely due to differences in the relative rates of diffusional transport between experiments at stationary electrodes, where planar diffusion is the only means of mass transport, and the SECM experiment. The rate of mass transport to the tip electrode in SECM is dependant on the rate of cycling (i.e. the tip-substrate distance) of the mediator species between the tip and substrate and thus effectively higher rates of mass transport will be present with SECM feedback than would be expected for mass transport by diffusion alone.⁶⁷ This allows the observation of kinetic effects with SECM under conditions that would be mass transport limited in a voltammetry experiment. It is this effective increase in mass transport that also makes SECM a useful technique for examining fast et kinetics.⁶⁷⁻⁶⁹ Another apparent anomaly is the difference in topography between the oxidized and unoxidized regions in fig. 2D. According to SECM positive feedback theory this change in current corresponds to a change in surface elevation of about 0.5 μm .⁷¹ It is likely that this difference is due to removal of carbon by the oxidation process.

Three dark spots on the oxidized regions of figs. 2A and 2B are also likely due to kinetic effects. An alternate explanation is that the spots correspond to pits in the oxidized region. If so, they would also show a decrease in tip current in figs. 2C and 2D, which in not

seen. Thus, the spots appear to be regions of lower et rate in the oxidized region that disappear as the rate is increased into the diffusion-limited regime.

Unexpected features also show up in the unoxidized region of the surface at lower applied potentials where the et rate is low. These features are clearly not topographic in nature since they do not appear in fig. 2D and are therefore likely due to local variations in the heterogeneous et rate on these surfaces. While the precise origin of these features is unclear, they could be due to naturally occurring oxides, variations in surface microstructure, or the presence of polishing debris. The use of SECM to locate and directly measure these variations in heterogeneous et at specific sites on GCE is the subject of a forthcoming publication.⁷²

As mentioned previously, several species show accelerated et rates on carbon electrodes following oxidation⁵⁻¹⁵ and are thus potential candidates for use as reaction-rate imaging mediators. McDermott et al. have shown that both the Eu(II/III) and V(II/III) systems in addition to Fe(II/III) are sensitive to the presence of surface oxides on carbon electrodes.¹⁴ In addition to the work presented here, we have also investigated the selective imaging of oxides on carbon electrode surfaces using the V(II)/V(III) redox couple. These experiments gave similar results but were technically more difficult due to complications from background processes at the tip electrode.⁷³

Local Oxidation of Glassy Carbon Surfaces by Micro-Reagent Mode SECM

Localized oxidation of the GCE surface is possible with the micro-reagent SECM mode, fig. 3. The tip electrode is placed close to the carbon surface and is then used to electrogenerate a strong oxidant. Initial experiments examined whether Ce(IV), which is a powerful oxidant

commonly used in coulometric titration and is easily generated by oxidation of Ce(III) at an SECM tip, could be used to locally oxidize carbon. However, experiments in which a GCE was soaked for various times in solutions containing different concentrations of the Ce(IV) ion showed no effect on the et rate for the Fe(II)/Fe(III) system.

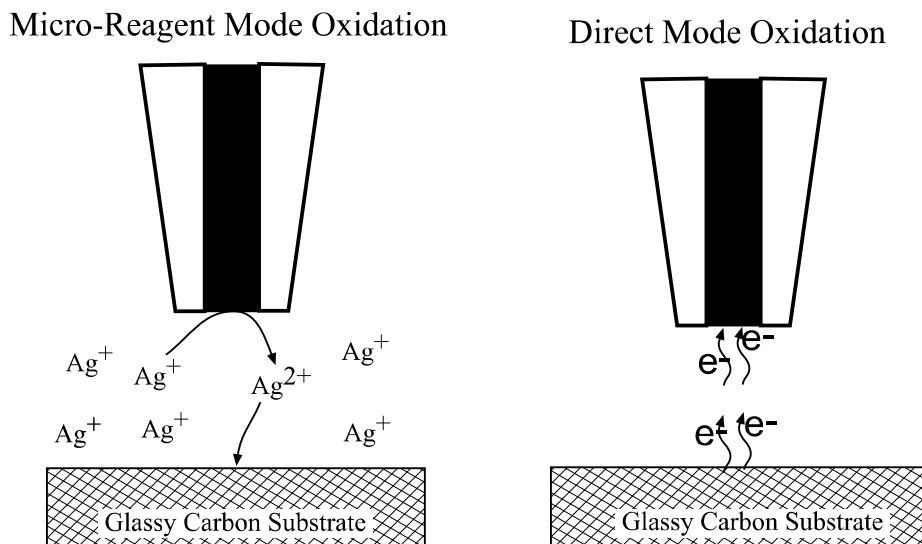


Fig. 3. Illustration of the two modes used for localized oxidation of the carbon surface by the SECM tip.

Ag(II) , with a formal potential of 1.71 V vs. Ag/AgCl (1-4 M HNO_3),⁷⁴ is a significantly stronger oxidizing agent than Ce(IV) ($E^0 = 1.41$ V vs. Ag/AgCl).⁷⁵ Davis and Lingane demonstrated the generation of Ag(II) at a gold electrode in 4 M nitric acid at 0 °C and successfully employed it as a coulometric titrant.⁷⁶ In less acidic solution, Ag(II) is rapidly reduced to Ag(I) by water.⁷⁷ However, since the SECM tip can generate reagents with a very small tip-substrate separation, unstable species can often be used for surface-modifications. At tip-separations of 1 μm or less, the diffusion time between tip and samples

is milliseconds or less. Thus, electrogenerated Ag(II) ion can possibly diffuse to and react with the carbon surface before undergoing solution-phase reduction to Ag(I).

Local oxidation of glassy carbon by tip-generated Ag(II) was attempted using a 12.7- μm dia. gold UME tip. Cyclic voltammetry at a gold UME tip clearly indicates a Ag(II) wave at around 1.75 V vs. Ag/AgCl in a solution of 2 mM silver nitrate in 1 M nitric acid. Ag(II) was generated by holding the UME tip at a constant potential of 1.85 V for approximately 30 s. The tip-substrate spacing for these experiments was set by starting electrogeneration of Ag(II) with the tip far from the substrate electrode surface. As the tip was moved towards the surface, a cathodic substrate current indicated that the substrate electrode was reducing the tip-generated Ag(II). The approach continued until the cathodic substrate current was approximately equal to the anodic tip current. This behavior indicated that the Ag(II) was sufficiently stable to diffuse to the substrate before reduction. After the localized oxidation was completed, the glassy carbon surface was analyzed by a separate reaction-rate experiment. Fig. 4 shows reaction-rate images of a glassy carbon surface with an oxidized region that was formed by the local generation of the Ag(II) ion. These reaction-rate images were collected with a 10- μm dia. Pt tip electrode in a solution of 2 mM $\text{Fe}(\text{ClO}_4)_3$ in 1 M sulfuric acid with substrate potentials at (A) 0.80, (B) 1.00 and (C) 1.20 V. The image collected at 0.80 V clearly shows a region of increased current due to catalysis of the et reaction for the Fe(II/III) system as compared to the regions not previously exposed to the Ag(II) ion during the original oxidation experiments. The kinetic origin of this current is further confirmed by images collected at 1.00 V and 1.20 V showing that as the rate of the et reaction approaches a mass transport limit, a topographically flat surface is observed. Note that the drift of about 25 μm in the y axis between scans is not sufficient to completely

remove the feature from the imaged region and so absence of the feature in fig. 4C cannot be ascribed to drift.

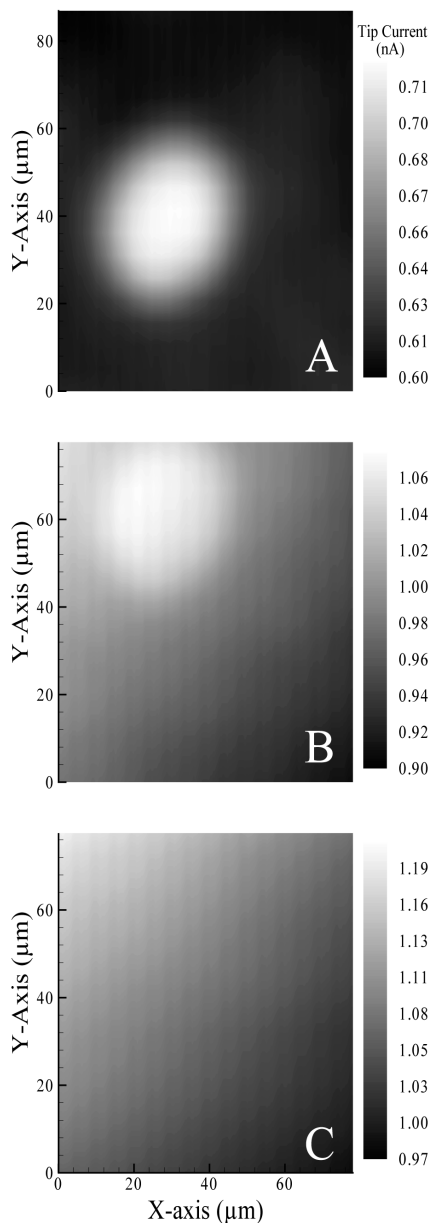


Fig. 4. SECM reaction-rate mode images of a spot of oxidized glassy carbon formed with the micro-reagent mode using Ag^{2+} . The conditions for the oxidation step are described in the text. The tip electrode was biased at 0.00 V while the substrate potentials for each image were (A) 0.80, (B) 1.00, and (C) 1.20 V vs. Ag/AgCl.

Production of larger patterns of surface oxidation by moving the tip during the generation of Ag(II) was found to be difficult. These experiments typically resulted in either no apparent oxidation or generation of oxidation patterns that did not correspond to that expected from the tip movement during patterning. We conjecture that the combination of diffusion of the Ag(II), its instability, and sensitivity to tip-substrate position produced poorly defined results.⁷³

Localized Oxidation of Carbon Electrode Surfaces by Direct Mode SECM

Modification by the direct mode was also used to produce localized regions of oxides on carbon surfaces. The direct mode uses the tip to direct current flow through the sample surface. This allows for a highly localized current flow and, thus, localized electrochemical modifications. A general schematic of the direct mode oxidation procedure is illustrated in fig. 3. With the tip electrode placed close to a glassy carbon electrode, a galvanostat was used to drive a predetermined current between the tip and substrate for a specific amount of time thereby allowing precise control over the amount of charge “injected” into the carbon surface. During current flow, solvent is reduced at the tip electrode and the carbon-electrode is oxidized.

Fig. 5 shows reaction-rate images of an oxidized region generated by direct mode modification. Oxidation was performed in a cell containing distilled-deionized water (18 M Ω /cm) using a 100- μ m dia. Pt tip electrode and a current of 46 μ A (0.58 A/cm²) applied between the tip and substrate for 5 s at a tip-to-substrate separation of \sim 1 μ m. Subsequent reaction-rate SECM images of the oxidized substrate were performed in a 2 mM solution of Fe(II) in 1 M H₂SO₄ with a 10- μ m dia. Pt tip electrode biased at 0.80 V. This data gives an example of reaction-rate imaging with the oxidation of Fe(II) occurring at the tip, which is

the opposite of the systems presented to this point. The substrate potential was held at (A) 0.243, (B) 0.043, (C) -0.243, and (D) -0.423 V, which corresponds to the reaction-rate region for the reduction of the tip generated Fe(III) as shown in fig. 1. As observed above, the region of higher current observed in fig. 5A disappears as overpotential increases. The dark spot that appears in all images appears to be an inactive area of the electrode surface. The feature is clearly not topographic. As discussed previously, topographic features give opposite responses in the positive and negative feedback mode. For example, if the observed feature were a pit, it would show increased current in the slow kinetic regime, which mimics the insulating substrate response. As the rate of et increased at the substrate, the surface would mimic positive feedback and a decrease in current at the pit would be observed. Since no change is observed in the appearance of this spot in the images at all potentials, it is assumed that it is a small inactive site on the electrode surface. This could be due to an impurity in the glassy carbon or a region of exposed basal plane carbon. It is unclear if this is a naturally occurring site or related to the oxidation treatment.

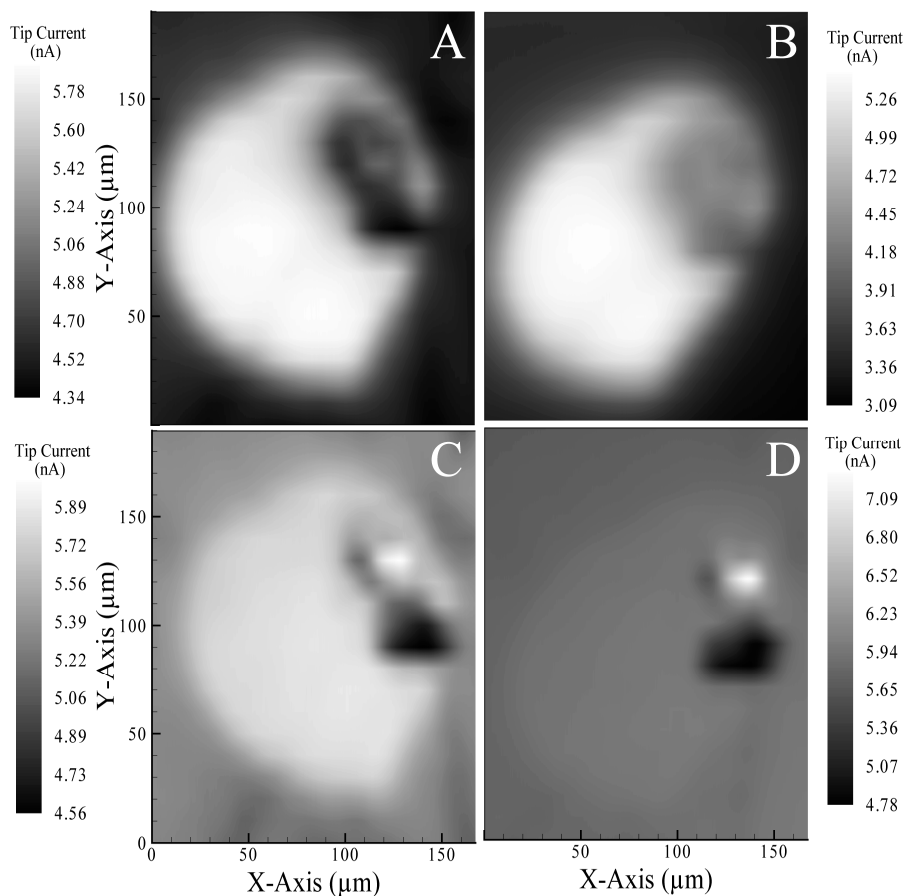


Fig. 5. SECM reaction-rate mode images of a region of oxidized carbon formed by the direct mode oxidation with a 100- μm dia. tip. The tip electrode was biased at 0.80 V while the substrate potentials for each image were (A) 0.243, (B) 0.043, (C) -0.243, and (D) -0.443 V vs. Ag/AgCl.

A smaller tip electrode allows the formation of more complex oxidation patterns and a demonstration of the reproducibility of the oxidation procedure. Fig. 6 shows the result of a series of localized oxidations performed with a 10 μm dia. Pt tip. Spots were generated by applying 0.46 μA (current density = 0.58 A/cm^2) for 5 s and the line was generated by moving the tip at 2 $\mu\text{m}/\text{s}$ while applying the same current density. The reaction-rate images

shown in fig. 6 were collected with a 10- μm dia. Pt tip in 2 mM Fe(II) perchlorate in 1 M sulfuric acid with substrate potentials of (A) 0.243, (B) 0.043, (C) -0.243, and (D) -0.423 V.

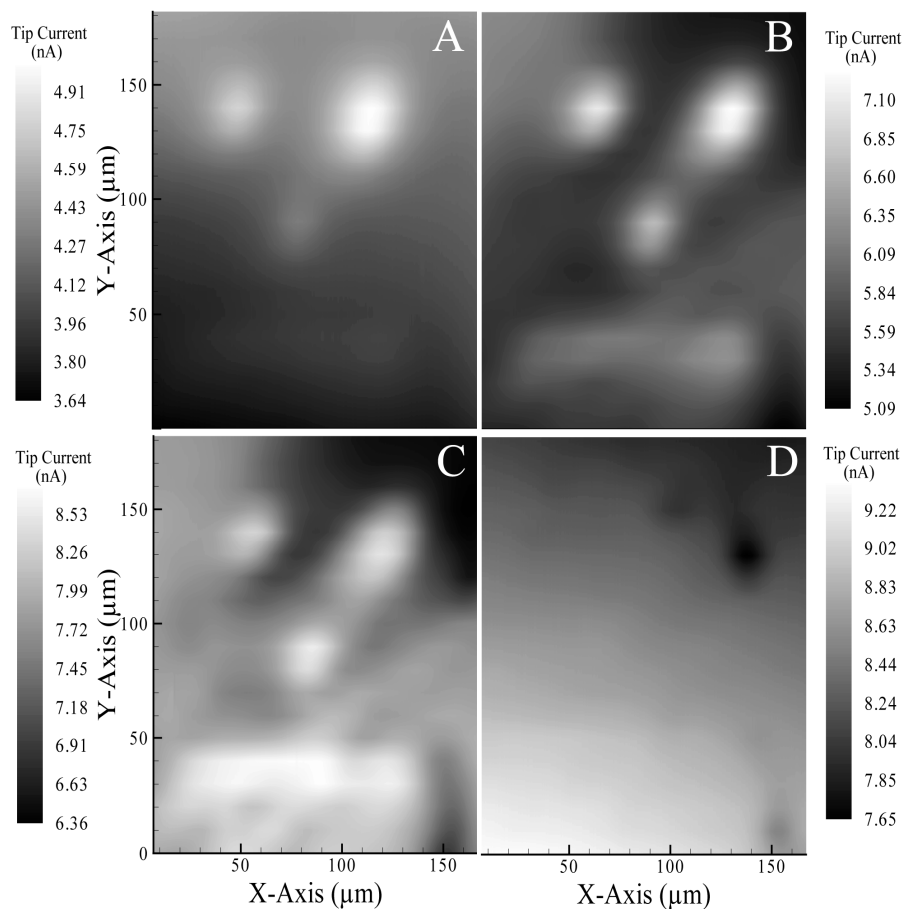


Fig. 6. SECM reaction-rate mode images of a pattern of oxidized spots and a line formed with the direct mode oxidation using a 10 μm -dia. tip. The oxidation procedure is described in the text. The tip electrode was biased at 0.80 V while the substrate potentials for each image were (A) 0.243, (B) 0.043, (C) -0.243, and (D) -0.443 V vs. Ag/AgCl.

The direct mode oxidation was found to be regularly reproducible as long as the experiments were performed in deionized water. Attempts to locally generate oxides with the direct mode in sulfuric and perchloric acids using the same current densities as in the

deionized water experiments showed no apparent effect on the carbon surface. We believe that the higher ionic strength of these solutions lead to a spreading of the current flow between the tip and substrate electrodes. Using higher current densities in sulfuric and perchloric acid produced an increase in the overall et rate for the GCE as indicated by cyclic voltammetry. This suggests that the oxidation was not confined to the tip region in the higher ionic strength solutions.

The effect of different current densities on the oxidation results obtained in deionized water was also investigated. Fig. 7 shows a photomicrograph (A) and a reaction-rate image (B) of a series of oxidized spots generated by applying current densities ranging from 0.014 A/cm² up to 0.35 A/cm². This current density range was at the threshold for local oxidation of the carbon surface. Current densities below this range resulted in no oxidation, while the higher current densities were still mild enough to avoid the surface corrosion and pitting that was observed in experiments at current densities of ~12 A/cm². Note that the oxidation leads to a change in the appearance of the carbon surface with the oxidized regions showing darker contrast as compared to the unoxidized; this was also observed with the larger spots (100 μm). This is probably due to a graphitic oxide layer.¹² The accompanying reaction-rate image shown in fig. 7 suggests an increase in the et rate for the more heavily oxidized regions. Fig. 7 was collected with a 10 μm Pt tip biased at 0.80 V vs. Ag/AgCl in a 2 mM solution of Fe(ClO₄)₂ in 1 M H₂SO₄ with a 0.043 V substrate potential. The increase in et rate can easily be seen by plotting the maximum tip current at each spot in fig. 7 versus the total “charge dose” injected during each oxidation as shown in fig. 8. The data point for a charge dose of zero was calculated as an average of several current values over unmodified regions. This figure demonstrates that an increased charge dose during the oxidation leads to a higher

rate of et at a given potential for the Fe(II/III) system. As charge dose during the oxidation experiment increases, the increase in tip current observed in the subsequent imaging experiment increases rapidly up to a charge dose of $\sim 0.5 \mu\text{C}$. Note that as the oxidation charge dose increases further, the effect on tip imaging current is less pronounced but not removed. This could be due to a local saturation of oxides in the modified region or surface damage occurring at the higher charge dose.

Conclusions

SECM methods have been introduced that allow the formation and characterization of patterns of oxides on glassy carbon surfaces. Compared to previous techniques for oxide characterization, this method allows for the direct visualization of the distribution of oxides on these surfaces without the need for derivatization.

Chemically specific imaging of oxides present on these surfaces was demonstrated by taking advantage of differential heterogeneous et rates for the Fe(II/III) reaction occurring at unoxidized and oxidized glassy carbon electrodes. Based on work by McCreery and coworkers^{7,8} the use of the Fe(II/III) system seems to point towards the presence of carbonyl groups following the oxidation treatment (although other carbon oxides cannot be ruled out) thereby adding another degree of chemical specificity to this technique.

The localized generation of surface oxides was demonstrated using both the micro-reagent and direct modification modes of SECM. The micro-reagent mode was used to perform a chemical oxidation of the surface by generating a strong oxidant at the UME tip while spaced close to the carbon surface. Exposure of the carbon surface to Ce(IV) did not significantly catalyze the et rate for the Fe(II/III) redox couple as has been shown to occur with other procedures known to form oxides on the surface. However, the use of the stronger

oxidant, Ag(II), allows oxidation of distinct sites on a carbon electrode surface. Experiments conducted at single sites on the surface appear to show control over the oxidation process, however the reproducibility of the technique was found to be insufficient to allow for a detailed study. The reason for this is unclear, but it is conjectured that the instability of Ag(II) in aqueous solution limits this technique.

In contrast, direct mode oxidation is a much more versatile route toward the generation of complex patterns of oxides on carbon surfaces. The reproducibility of the technique was found to depend on solution resistance in that high conductivity solutions (i.e. perchloric and sulfuric acids) led to poor localization. Direct mode oxidation also allows more complicated studies of the oxidation process by giving an easy way to control the “charge dose” of the oxidation procedure. This can be done directly by changing either the current or the length of time for the oxidation procedure. “Charge dose” studies followed with reaction-rate imaging qualitatively show that the et rate for the Fe(II/III) system scales with the amount of charge “injected” in each oxidation experiment possibly indicating a correlation between surface oxide density and et rate. A forthcoming publication will describe experiments to quantitatively study the effect of localized oxidation on the et kinetics for the Fe(II/III) species.⁷²

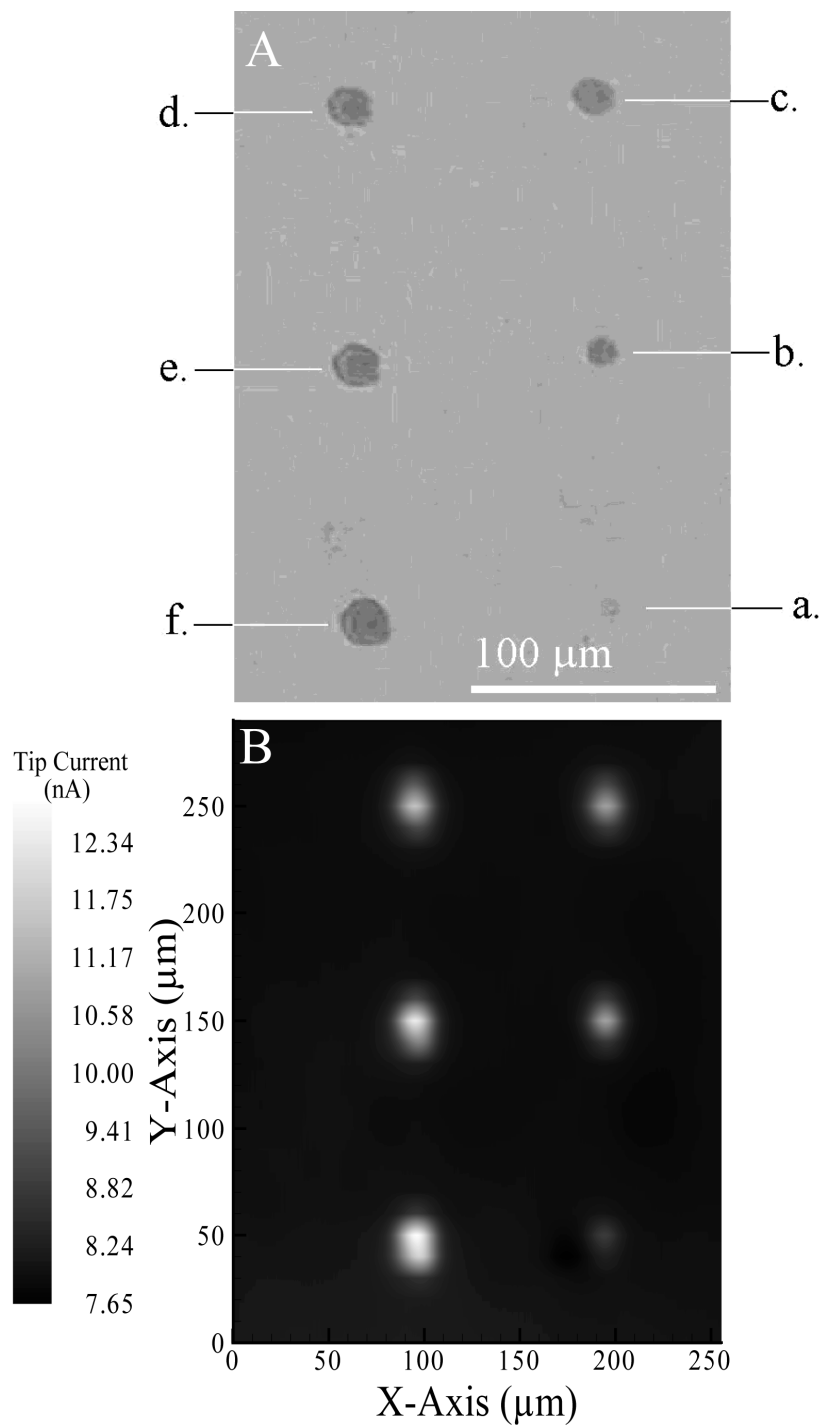


Fig. 7. Photomicrograph (A) and SECM reaction-rate image (B) of a series of oxidized spots formed by direct-mode oxidation using the following current densities at each labeled spot: (a) 0.014, (b) 0.07, (c) 0.14, (d) 0.21, (e) 0.28, and (f) 0.35 A/cm².

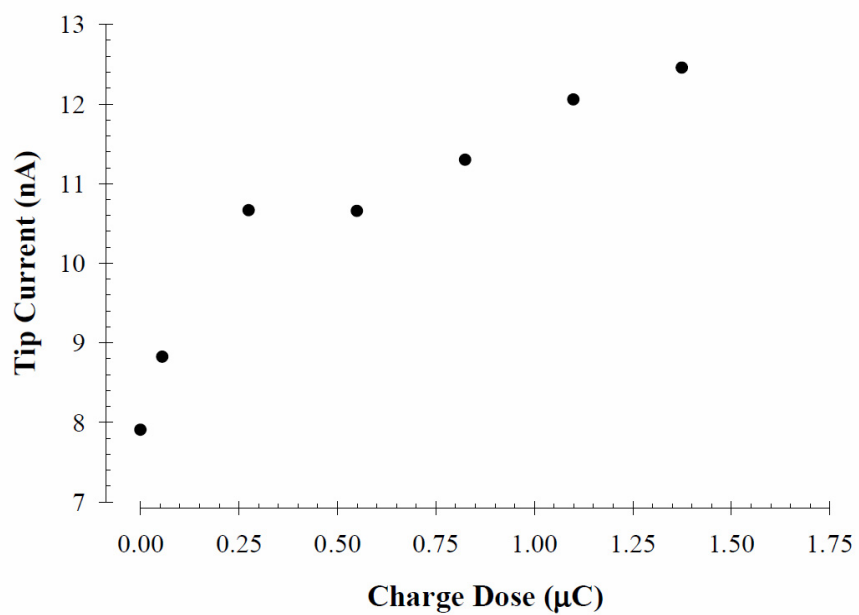


Fig. 8. Plot of measured tip current over each spot in the SECM image shown in fig. 7 versus the total charge “injected” in the oxidation step performed at each spot.

Acknowledgments

The National Science Foundation (CHE-94144101) supported this work.

References

1. P. Pantano, T. H. Morton and W. G. Kuhr, *J. Am. Chem. Soc.*, **113**, 1832 (1991).
2. K. M. Millan, A. J. Spurmanis and S. R. Mikkelsen, *Electroanalysis*, **4**, 929 (1992).
3. J. R. Lenhard and R. W. Murray, *J. Am. Chem. Soc.*, **100**, 7870 (1978).
4. P. Bianco, J. Haladjian and C. Bourdillon, *J. Electroanal. Chem.*, **293**, 151 (1990).
5. D. C.-S. Tse and T. Kuwana, *Anal. Chem.*, **50**, 1315 (1978).
6. F. A. Armstrong, A. M. Bond, H. A. O. Hill, B. N. Olive and I. S. M. Psalti, *J. Am. Chem. Soc.*, **111**, 9185 (1989).
7. P. H. Chen, M. A. Fryling and R. L. McCreery, *Anal. Chem.*, **67**, 3115 (1995).
8. P. H. Chen and R. L. McCreery, *Anal. Chem.*, **68**, 3958 (1996).
9. R. C. Engstrom, *Anal. Chem.*, **54**, 2310 (1982).
10. R. C. Engstrom and V. A. Strasser, *Anal. Chem.*, **56**, 136 (1984).
11. J. F. Evans and T. Kuwana, *Anal. Chem.*, **49**, 1632 (1977).
12. L. J. Kepley and A. J. Bard, *Anal. Chem.*, **60**, 1459 (1988).
13. R. L. McCreery, K. K. Cline, C. A. McDermott and M. T. McDermott, *Colloids Surf. A*, **93**, 211 (1994).
14. C. A. McDermott, K. R. Kneten and R. L. McCreery, *J. Electrochem. Soc.*, **140**, 2593 (1993).
15. R. J. Taylor and A. A. Humffray, *J. Electroanal. Chem.*, **42**, 347 (1973).
16. G. E. Cabaniss, A. A. Diamantis, J. Murphy, W.R., R. W. Linton and T. J. Meyer, *J. Am. Chem. Soc.*, **107**, 1845 (1985).
17. J. Harvey, C. Koslowski and P. M. A. Sherwood, *J. Mat. Sci.*, **22**, 1581 (1987).
18. A. Proctor and P. M. A. Sherwood, *Carbon*, **21**, 53 (1983).
19. T. Wang and P. M. A. Sherwood, *Chem. Mat.*, **7**, 1020 (1995).

20. T. Wang and P. M. A. Sherwood, *Chem. Mat.*, **7**, 1031 (1995).
21. Y. Xie and P. M. A. Sherwood, *Appl. Spec.*, **44**, 1621 (1990).
22. Y. Xie and P. M. A. Sherwood, *Appl. Spec.*, **45**, 1158 (1991).
23. M. A. Fryling, J. Zhao and R. L. McCreery, *Anal. Chem.*, **67**, 967 (1995).
24. K. G. Ray and R. L. McCreery, *Anal. Chem.*, **69**, 4680 (1997).
25. K. G. Ray and R. L. McCreery, *J. Electroanal. Chem.*, **469**, 150 (1999).
26. P. Pantano and W. G. Kuhr, *Anal. Chem.*, **63**, 1413 (1991).
27. P. Pantano and W. G. Kuhr, *Anal. Chem.*, **65**, 2452 (1993).
28. P. Hopper and W. G. Kuhr, *Anal. Chem.*, **66**, 1996 (1994).
29. A. J. Bard and M. V. Mirkin, *Scanning Electrochemical Microscopy*, p. 650, Marcel Dekker, Inc., New York, (2001).
30. A. J. Bard, F.-R. F. Fan and M. V. Mirkin, in *Electroanalytical Chemistry*, A. J. Bard, Editor, Vol. 18, p. 243, (1994).
31. A. L. Barker, M. Gonsalves, J. V. Macpherson, C. J. Slevin and P. R. Unwin, *Anal. Chim. Acta*, **385**, 223 (1999).
32. M. V. Mirkin and B. R. Horrocks, *Anal. Chim. Acta*, **406**, 119 (2000).
33. D. O. Wipf and A. J. Bard, *J. Electrochem. Soc.*, **138**, L4 (1991).
34. M. A. Alpuche-Aviles and D. O. Wipf, *Anal. Chem.*, **73**, 4873 (2001).
35. K. Borgwarth, D. G. Ebling and J. Heinze, *Ber. Bunsen-Ges. Phys. Chem.*, **98**, 1317 (1994).
36. P. I. James, L. F. Garfias-Mesias, P. J. Moyer and W. H. Smyrl, *J. Electrochem. Soc.*, **145**, L64 (1998).
37. M. Ludwig, C. Kranz, W. Schuhmann and H. E. Gaub, *Rev. Sci. Instrum.*, **66**, 2857 (1995).
38. D. O. Wipf, A. J. Bard and D. E. Tallman, *Anal. Chem.*, **65**, 1373 (1993).
39. J. V. Macpherson and P. R. Unwin, *Anal. Chem.*, **73**, 550 (2001).
40. D. H. Angell and T. Dickinson, *J. Electroanal. Chem.*, **35**, 55 (1972).
41. J.-M. Kauffmann, A. Laudet, G.-J. Patriarche and G. D. Christian, *Talanta*, **29**, 1077 (1982).

42. G. Wittstock, H. Emons, M. Kummer, J. R. Kirchhoff and W. R. Heineman, *Fresenius' J. Anal. Chem.*, **348**, 712 (1994).
43. G. Wittstock, R. Hesse and W. Schuhmann, *Electroanalysis*, **9**, 746 (1997).
44. S. Jayaraman and A. C. Hillier, *Langmuir*, **17**, 7857 (2001).
45. K. Jambunathan, B. C. Shah, J. L. Hudson and A. C. Hillier, *J. Electroanal. Chem.*, **500**, 279 (2001).
46. B. C. Shah and A. C. Hillier, *J. Electrochem. Soc.*, **147**, 3043 (2000).
47. G. Wittstock, *Fresenius' J. Anal. Chem.*, **370**, 303 (2001).
48. J. Zaumseil, G. Wittstock, S. Bahrs and P. Steinrucke, *Fresenius' J. Anal. Chem.*, **367**, 352 (2000).
49. D. T. Pierce, P. R. Unwin and A. J. Bard, *Anal. Chem.*, **64**, 1795 (1992).
50. D. T. Pierce and A. J. Bard, *Anal. Chem.*, **65**, 3598 (1993).
51. W. B. Nowall, D. O. Wipf and W. G. Kuhr, *Anal. Chem.*, **70**, 2601 (1998).
52. D. Mandler and A. J. Bard, *J. Electrochem. Soc.*, **137**, 1079 (1990).
53. J. Zhou and D. O. Wipf, *J. Electrochem. Soc.*, **144**, 1202 (1997).
54. C. Kranz, M. Ludwig, H. E. Gaub and W. Schuhmann, *Advan. Mater.*, **7**, 38 (1995).
55. C. Kranz, H. E. Gaub and W. Schuhmann, *Advan. Mater.*, **8**, 634 (1996).
56. F. Ge, R. C. Tenent and D. O. Wipf, *Anal. Sci.*, **17**, 27 (2001).
57. R. L. McCreery, in *Electroanalytical Chemistry*, Vol. 17, p. 221, Marcel-Dekker, Inc., New York, (1991).
58. I. F. Hu, D. H. Karweik and T. Kuwana, *J. Electroanal. Chem.*, **188**, 59 (1985).
59. D. J. Ives and G. J. Janz, *Reference Electrodes: Theory and Practice*, Academic Press, New York, (1961).
60. R. M. Wightman and D. O. Wipf, in *Electroanalytical Chemistry*, A. J. Bard, Editor, Vol. 15, p. 267, Marcel Dekker, New York, (1989).
61. D. O. Wipf and A. J. Bard, *J. Electrochem. Soc.*, **138**, 469 (1991).
62. D. O. Wipf, *Colloids Surf., A*, **93**, 251 (1994).
63. D. O. Wipf, in *Scanning Electrochemical Microscopy*, A. J. Bard and M. V. Mirkin, Editors, p. 61, John Wiley & Sons, New York, (2001).

64. C. Barbero, J. J. Silber and L. Sereno, *J. Electroanal. Chem.*, **248**, 321 (1988).
65. A. J. Bard and L. Faulkner, *Electrochemical Methods*, 2nd ed., John Wiley & Sons, Inc., New York, (2001).
66. A. J. Bard, M. V. Mirkin, P. R. Unwin and D. O. Wipf, *J. Phys. Chem.*, **96**, 1861 (1992).
67. A. J. Bard, F. R. F. Fan, J. Kwak and O. Lev, *Anal. Chem.*, **61**, 132 (1989).
68. M. V. Mirkin, L. O. S. Bulhoes and A. J. Bard, *J. Am. Chem. Soc.*, **115**, 201 (1993).
69. M. V. Mirkin and A. J. Bard, *J. Electrochem. Soc.*, **139**, 3535 (1992).
70. M. V. Mirkin, T. C. Richards and A. J. Bard, *J. Phys. Chem.*, **97**, 7672 (1993).
71. J. Kwak and A. J. Bard, *Anal. Chem.*, **61**, 1221 (1989).
72. R. C. Tenent and D. O. Wipf, *manuscript in preparation*, , .
73. R. C. Tenent, Ph.D. Thesis, *Localized Modification and Studies of Carbon Electrode Surfaces by Scanning Electrochemical Microscopy*, Mississippi State University, Mississippi State, (2000).
74. A. A. Noyes and A. Kossiakoff, *J. Am. Chem. Soc.*, **57**, 1238 (1935).
75. A. J. Bard, R. Parsons and J. Jordan, *Standard Potentials in Aqueous Solution*, Marcel Dekker, Inc., New York, (1985).
76. D. G. Davis and J. J. Lingane, *Anal. Chim. Acta*, **18**, 245 (1958).
77. A. A. Noyes, J. L. Hoard and K. S. Pitzer, *J. Am. Chem. Soc.*, **57**, 1221 (1935).